20th Australasian Fluid Mechanics Conference
Perth, Australia
5-8 December 2016

Fluid-structure Interactions of Unconstrained Spheres Rolling Down an Incline

F. Y. Houdroge[1], T. Leweke[2], M. C. Thompson[1] and K. Hourigan[1]

[1]FLAIR, Department of Mechanical and Aerospace Engineering
Monash University, Victoria 3800, Australia

[2]IRPHE UMR 7342, CNRS
Aix-Marseille Université, Centrale Marseille, 13384 Marseille, France

Abstract

A numerical investigation of the flow structure and the fluid forces associated with a sphere rolling down an inclined plane with no constrains is undertaken. The Reynolds numbers considered are in the range $18-315$. The study shows that the mirror symmetry of vortex shedding is broken as the Reynolds number is increased, leading to a side-to-side motion of the sphere.

Introduction

At low Reynolds numbers, the flow around a stationary sphere placed in an unbounded flow remains steady and attached until $\mathrm{Re} \approx 20$ [2]. When the flow separates, the recirculation zone in the wake remains symmetric about the streamwise centreline of the sphere [3]. At $\mathrm{Re} \approx 210$, the flow undergoes a transition to steady asymmetric flow [4, 5] which is characterised by the development of a two-tailed wake. At $270 < \mathrm{Re} < 280$, a periodic undulation in the asymmetric wake is observed, which triggers the onset to unsteady flow via a supercritical Hopf bifurcation [3, 4, 6]. As Re increases, fully formed vortices shed into the wake of the sphere that take the form of vortex 'hairpins'. The flow also maintains a planar symmetry until $\mathrm{Re} > 350$ [7].

Amongst the studies conducted on rotating spheres near boundaries are Zeng *et al.*'s [8] and Cherukat & McLaughlin's [10] works (the latter being restricted to the Stokes regime), where a sphere is moving near a wall (but not *on* it) at a gap of the order of 0.75 sphere diameters or greater. Their results indicate that, in general, any observed rotation has been in the prograde direction and that the free rotation has little effect on the lift and drag forces. The transition to the two-tailed wake occurs at lower Re than for that of an isolated sphere, and this transition also depends on the distance to the wall. The unsteady flow takes the form of hairpin vortices and loops in the wake. Zeng *et al.* [8] describe that the wall has two effects on the flow structure: the first is a viscous one acting to delay the transition to unsteady flow, and the second tends to stabilise the flow and is due to the asymmetry in the wake. Verekar & Arakeri [11] have undertaken a study where a sphere is freely rolling on an inclined plane, focusing mainly on the physics behind the flow features and the forces acting on the sphere. However, an analysis of the wake transitions and induced motion of the body were not investigated.

More recent studies have looked at the stability of the wake and the dynamics of the flow around spheres translating and rotating very close to a wall [1,9,12] at moderate Reynolds numbers (of order 10^{1-3}, covering both steady and unsteady regimes). These studies show that the wall and the imposed body rotation have a great impact on the wake structures and instabilities. For $\alpha > 0$, where $\alpha = a\omega/U$ is the non-dimensional rotation rate of the body, a compact zone of recirculating fluid is created and the unsteady flow is marked by the shedding of hairpin vortices. For $\alpha < 0$, a stream-wise vortex pair appears in the wake and as Re is increased, the wake undergoes a transition to an antisymmetric mode.

In this study, we look at the fluid-structure interaction of an unconstrained sphere rolling on an inclined surface, focusing mainly on the body forces, the movement of the sphere and the development and structure of the flow. The range of Reynolds numbers considered is 18–315. As a reference, some results of the rolling sphere at $\alpha = 1$ are also included.

Problem Definition and Methodology

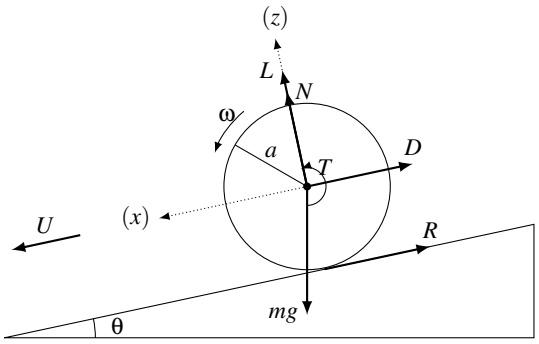

Figure 1: Two-dimensional schematic of the configuration.

The rolling sphere setup is illustrated in figure 1: U and ω represent the translational and angular velocities of the sphere respectively, T the torque, θ the inclination angle of the wall, L and D the lift and drag forces, N and R the components of the reaction force and mg the body's weight. The frame of reference is attached to the centre of the sphere here.

This problem requires a coupling between the equations of motions of the fluid (the continuity and Navier–Stokes equations) and the equation of motion of the sphere (Newton's second law).

Fluid equations

Let $\mathbf{u}(x, y, z, t) = (u, v, w)$ represent the velocity of the fluid. In the case of an incompressible flow, the continuity equation is:

$$\nabla \cdot \mathbf{u} = 0, \tag{1}$$

and the Navier–Stokes equation in an accelerating frame is:

$$\frac{\partial \mathbf{u}}{\partial t} + \mathbf{u} \cdot \nabla \mathbf{u} = -\frac{1}{\rho_f} \nabla P + \nu \nabla^2 \mathbf{u} - \frac{\mathrm{d}\mathbf{u_s}}{\mathrm{d}t}, \tag{2}$$

where $\mathbf{u_s}(x, y, z, t) = (u_s, v_s, 0)$ is the velocity of the sphere, ρ_f and ν the density and viscosity of the fluid respectively, and P the pressure field.

Body acceleration equations

The torque balance equation:

$$\sum \boldsymbol{\tau} = \frac{\mathrm{d}\mathbf{L}}{\mathrm{d}t} \quad (3)$$

$$\mathbf{T} + \mathbf{r} \wedge \mathbf{F_R} = \frac{2}{5} m a^2 \boldsymbol{\omega} \quad (4)$$

combined with a no-slip condition at the point of contact between the sphere and the wall allows the reaction force R to be expressed in terms of the sphere's angular velocity $\boldsymbol{\omega}$.

The x– and y–components of the sphere's acceleration $\mathbf{a}$ can thus be expressed using Newton's second law:

$$m\,\mathbf{a} = m\frac{\mathrm{d}\mathbf{u_s}}{\mathrm{d}t} = \sum \mathbf{F}, \quad (5)$$

where $\sum \mathbf{F}$ is the sum of all forces exerted on the sphere, giving

$$\ddot{x} = \frac{5}{7}\left[\left(1 - \frac{1}{\beta}\right) g \sin\theta - \frac{3D_x}{4\pi a^3 \rho_s} - \frac{3T_y}{4\pi a^4 \rho_s}\right] \quad (6)$$

and

$$\ddot{y} = \frac{15}{28\pi a^3 \rho_s}\left(D_y + \frac{T_x}{a}\right) \quad (7)$$

where $\beta = \rho_s/\rho_f$ is the ratio of the body density to the density of the fluid. The z-component of the acceleration, assuming the body stays in contact with the surface and does not lift-off, gives the following condition on the normal and lift forces: $N = m^* g \cos\theta - L$ where $m^* = 4/3\pi a^3(\rho_s - \rho_f)$.

Numerical formulation and validation

The code used for the numerical simulations uses a spectral element approach with iterative time-splitting. The solver has been tested, validated and used extensively in the past for similar problems and geometries [5,12,13,14,15,16], the main addition here being that the dynamics of the flow and the motion of the sphere are solved in a fully coupled way.

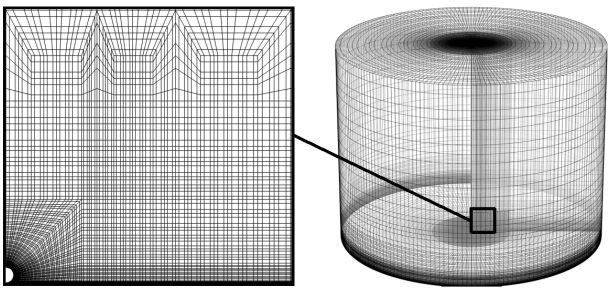

Figure 2: *Left*: two-dimensional mesh configuration in the vicinity of the sphere. *Right*: three-dimensional axisymmetric geometry and mesh.

The two-dimensional mesh, which is a of a finer resolution than the one that has been used and tested for convergence by Stewart *et al.* in the past [1], has an increased resolution of the macro-elements near the sphere region and can be seen on the left of figure 2. For the three-dimensional space, shown on the right of figure 2, the two-dimensional mesh is expanded into 192 Fourier planes around the symmetry axis located perpendicular to the bottom wall through the centre of the sphere.

In this study, the inclination angle of the wall θ and the density ratio β are both fixed at 5.8° and 2.2, respectively, and the viscosity of the fluid ν (or, equivalently, the Reynolds number) is varied throughout. The majority of the presented results are scaled for simplicity and clarity.

Results

Velocity of the sphere and frequency of oscillations

At low Reynolds numbers, the wake is steady and is characterised by the formation of two streamwise vortices, comparable to the twin-tailed structure that is observed behind a sphere in an unbounded flow. This effect can be seen on figure 3 at Re = 133, where a top view of the cross-stream vorticity isosurface is visualised (the sphere is located at the far left). The *red* and *blue* correspond to clockwise and anti-clockwise rotations respectively. The sphere in the final state is rolling along the wall at a constant terminal velocity.

When the flow becomes unsteady past Re ≈ 160, hairpin vortices start to shed periodically initially and the structure maintains a plane of symmetry that passes through the centre of the sphere perpendicular to the wall (figure 3 at Re = 186). The fluctuating forces affiliated with this state cause the body to develop a regular transverse oscillation, however, as the Reynolds number increases, the shedding becomes unstructured and irregular (figure 3 at Re = 223) eventually causing the mirror symmetry in the wake to break and large scale oscillations of the body to occur (figure 6 at Re = 267).

Overall, there is an increase in the mean velocity of the sphere with the Reynolds number (figure 4, top), and the Strouhal number $St = 2af/\overline{U}$, where f is the frequency of oscillation, remains constrained between 0.08 and 0.14 (figure 4, bottom). The latter is compared to the one obtained from the reference case where the sphere is rolling at a constant scaled velocity $U^* = 1$ and rotation rate $\alpha = 1$ in red (▲), and the results show overall good agreement with the slight deviation at Re = 250 and 300 due to the irregularity of the oscillations when the body is free to roll.

Trajectory of the sphere and corresponding flow structure

Figures 5 and 6 show the cross-stream component of the sphere's position in time at Re = 160 (around the transition to unsteady flow) and 267, respectively. The asymmetrical wake causes a deviation of the body across the y-axis. At low Reynolds numbers (below and around the transition), strong wake vortices shed initially very close to the sphere's surface, causing immediate strong oscillations of the body. The length of the wake then increases and the shedding grows weaker, leading to either a steady state (figure 3 at Re = 133) or a more sparse shedding (figure 5).

At higher Reynolds number, a transverse undulation of the wake becomes apparent and significant. The combined effect with the shedding of vortices causes the body's trajectory to exhibit very large and irregular deviations and oscillations. A visualisation of the flow and the wake undulations can clearly be seen on figures 6 and 7.

Force measurements

The mean drag and lift force coefficients, defined by:

$$\overline{C}_D = \left(\frac{2}{\pi a^2 \rho_f \overline{U}^2}\right) D \quad \text{and} \quad \overline{C}_L = \left(\frac{2}{\pi a^2 \rho_f \overline{U}^2}\right) L, \quad (8)$$

are consistent with the ones obtained through the reference case simulations (figure 8). The drag sees an overall decrease with the Reynolds number, and the lift a slight decrease until transition, after the which it slowly starts to increase again.

Conclusions

In the range of Reynolds numbers considered in this study, good

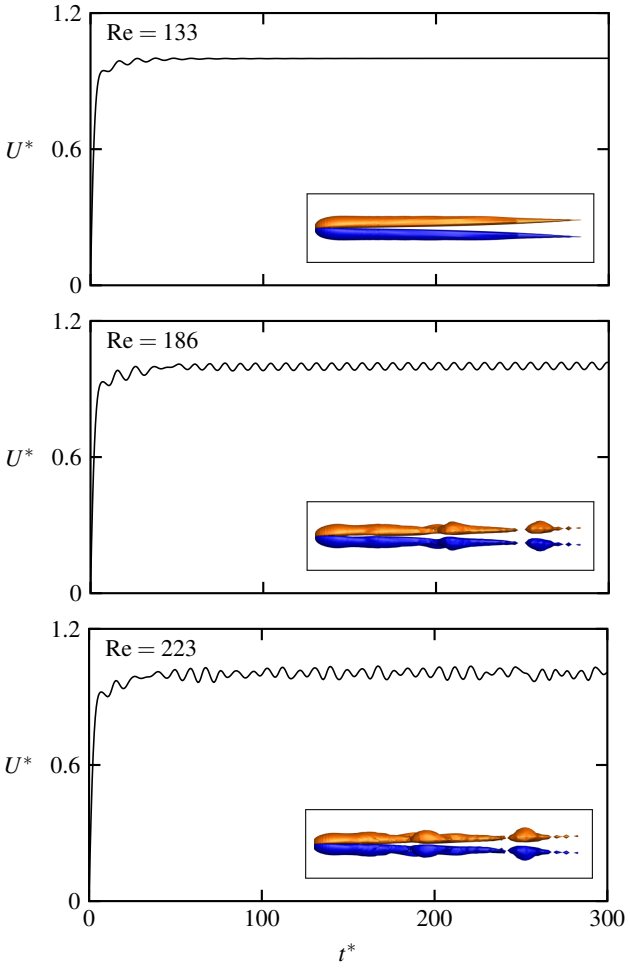

Figure 3: Variation of the velocity amplitude of the sphere in time. The images show the isosurfaces of the cross-stream vorticity field at the final state (taken here at $t^* = 300$) viewed from the top. The velocity is scaled by $\overline{U}$ and the time by $d/\overline{U}$.

qualitative agreement has been found between the reference case of a fixed rolling sphere at $\alpha = 1$ and the freely rolling sphere. The Strouhal number is comprised between 0.08 and 0.14, the mean drag coefficient decreases as the Reynolds number increases and the lift coefficient decreases then increases after the flow transitions. Altogether, the variations in the drag and lift coefficients between Re = 18 and 315 are of the order of 80% and 20%, respectively.

Below the transition to unsteady flow, the velocity of the body reaches a constant terminal state and the body rolls in a straight line often deviated from the $y = 0$ axis defined from the sphere's initial position. This is due to the fact that in the initial development of the flow, the sudden acceleration of the sphere causes a strong and compact shedding vortices which quickly subsides, thus altering the movement of the sphere. Past the transition to vortex shedding, the velocity and movement of the sphere become affected by the oscillating body forces. The developed response is, for Reynolds numbers close to the transition, a periodic oscillating one, and for higher Reynolds numbers an irregular and unstructured one characterised by large and asymmetrical oscillations. In general, the mean velocity of the sphere grows with the Reynolds number.

Acknowledgements

This research was supported under Australian Research Council, Discovery Projects funding scheme DP130100822 and DP150102879. We also acknowledge computing time support through National Computational Infrastructure projects D71 and N67.

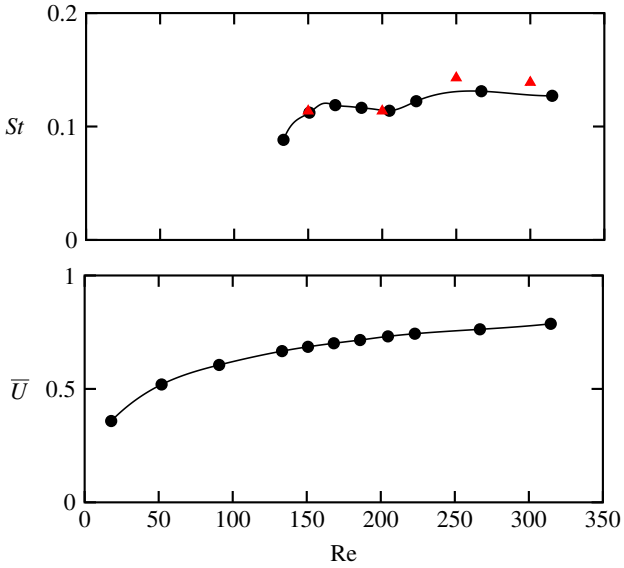

Figure 4: *Top*: plot of the Strouhal number $St = 2af/\overline{U}$ as a function of the Reynolds number. The black circles —●— represent the results from the freely rolling sphere simulations, and the red triangles ▲ the ones from the reference case ($\alpha = 1$). In the freely rolling case, the Reynolds number is based on the mean terminal velocity ($\mathrm{Re} = 2a\overline{U}/\nu$). *Bottom*: plot of the mean velocity of the sphere in the final state of the flow versus the Reynolds number.

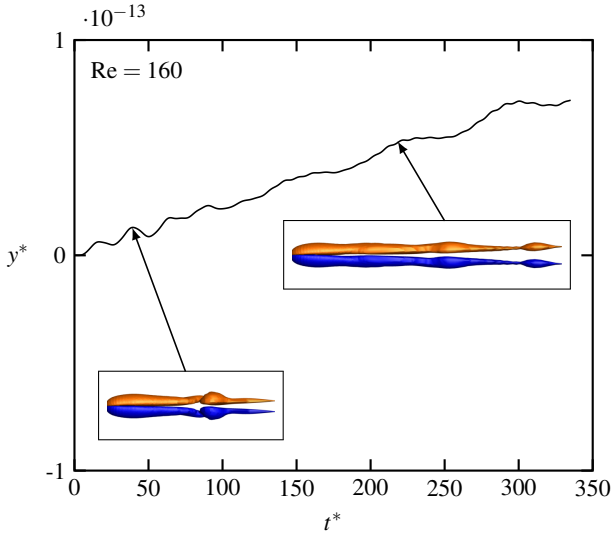

Figure 5: Re = 160: temporal evolution of the cross-stream component of the sphere's position, with y and t scaled by $2a$ and $d/\overline{U}$, respectively. The images show the isosurface of the cross-stream vorticity field at $t^* = 39$ and 218 (the sphere is located at the far left).

References

[1] Stewart, B.E. and Thompson, M.C. and Leweke, T. and Hourigan, K., Numerical and experimental studies of the rolling sphere wake. *J. Fluid Mech.*, **643**, 2010, 137–162.

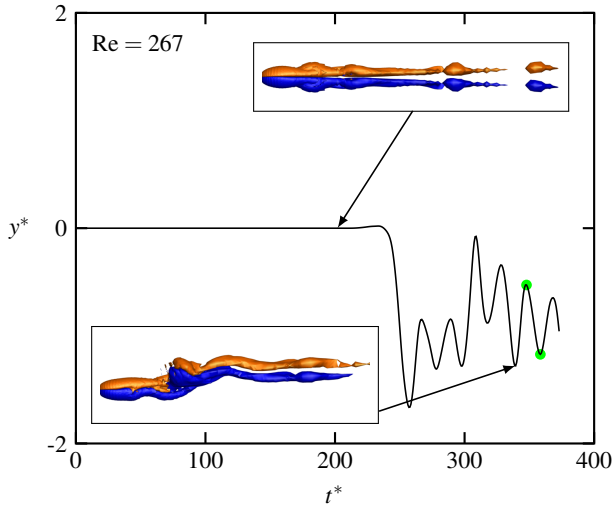

Figure 6: Re = 267: temporal evolution of the cross-stream component of the sphere's position, with y and t scaled by $2a$ and $d/\overline{U}$, respectively. The images show the isosurface of the cross-stream vorticity field at $t^* = 202$ and 340. The visualisation of the flow at the following two peaks (represented by the two green dots) is shown on figure 7.

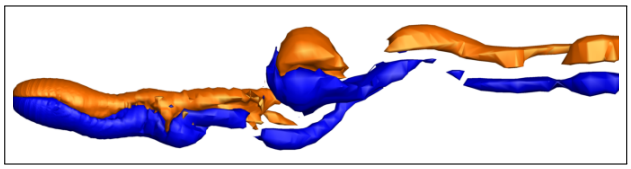

(a) Re = 267 at $t^* = 347.8$.

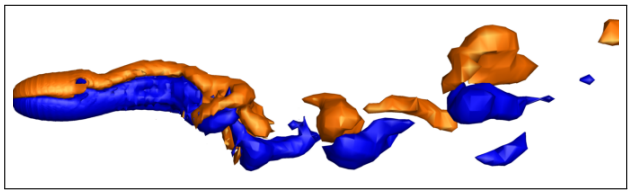

(b) Re = 267 at $t^* = 358.5$.

Figure 7: Re = 267: isosurface of the cross-stream vorticity field at two different positions of the sphere, represented by the green dots on figure 6.

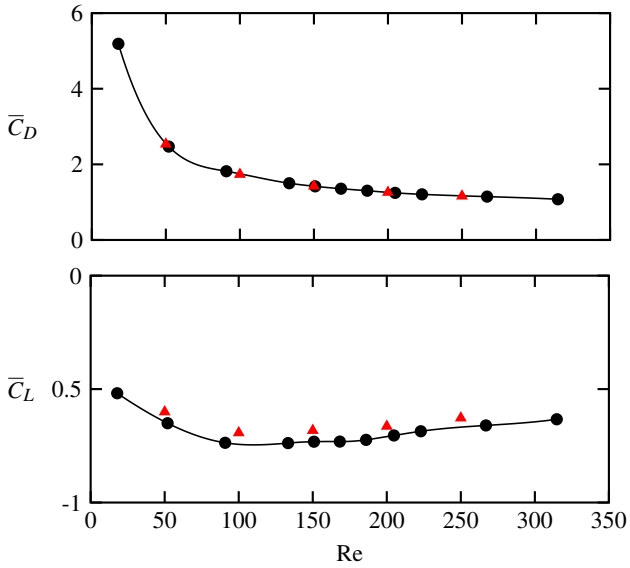

Figure 8: Plots of the mean drag and lift coefficients versus the Reynold number. The legend follows that of figure 4.

[2] Pruppacher, H. R. and Le Clair, B. P. and Hamielec, A. E., Some relations between drag and flow pattern of viscous flow past a sphere and a cylinder at low and intermediate reynolds numbers. *J. Fluid Mech.*, **44**, 1970, 781–790.

[3] Taneda, S., Experimental investigation of the wake behind a sphere at low Reynolds numbers. *J. Phys. Soc. Jpn.*, **11** (10), 1956, 1104–1108.

[4] Magarvey, R. H. and Bishop, R. L. Transition ranges for three-dimensional wakes. *Can. J. Phys.*, **39** (10), 1961, 1418–1422.

[5] Thompson, M. C. and Leweke, T. and Provansal, M., Kinematics and dynamics of sphere wake transition. *Journal of Fluids and Structures*, **15**, 2001, 575–586.

[6] Schouveiler, L. and Provansal, M., Self-sustained oscillations in the wake of a sphere. *Phys. Fluids*, **14** (11), 2002, 3846–3854.

[7] Mittal, S., Flow past rotating cylinders: effect of eccentricity. *J. Appl. Mech.*, **68** (4), 2000, 543–552.

[8] Zeng, L. and Balachandar, S. and Fischer, P., Wall-induced forces on a rigid sphere at finite reynolds number. *J. Fluid Mech.*, **536**, 2005, 1–25.

[9] Zeng, L. and Najjar, F. and Balachandar, S. and Fischer, P., Forces on a finite-sized particle located close to a wall in a linear shear flow. *Phys. Fluids*, **21** (3), 2009.

[10] Cherukat, P. and Mclaughlin, J. B., The inertial lift on a rigid sphere in a linear shear flow field near a flat wall. *J. Fluid Mech.*, **263**, 1994, 1–18.

[11] Verekar, P. K. and Arakeri, J. H., Sphere rolling down an incline submerged in a liquid. In *Proceedings of the 37th International & 4th National Conference on Fluid Mechanics and Fluid Power*, IIT Madras, Chennai, India, December 16-18 2010.

[12] Rao, A. and Passaggia, P. Y. and Bolnot, H. and Thompson, M. C. and Leweke, T. and Hourigan, K., Transition to chaos in the wake of a rolling sphere. *J. Fluid Mech.*, **695**, 2012, 135–148.

[13] Thompson, M. C. and Leweke, T. and Williamson, C. H. K., The physical mechanism of transition in bluff body wakes. *J. Fluids Struct.* **15**, 2001, 607–616.

[14] Ryan, K. and Thompson, M. C. and Hourigan, K., Three-dimensional transition in the wake of bluff elongated cylinders. *J. Fluid Mech.* **538**, 2005, 1–29.

[15] Rao, A. and Stewart, B. E. and Thompson, M. C. and Leweke, T. and Hourigan, K., Flows past rotating cylinders next to a wall. *J. Fluids Struct.* **27** (5–6), 2011, 668–679.

[16] Thompson, M. C. and Hourigan, K. and Cheung, A. and Leweke, T., Hydrodynamics of a particle impact on a wall. *Appl. Math. Modell.* **30** (11), 1356–1369.